Nanoscale

Accepted Manuscript

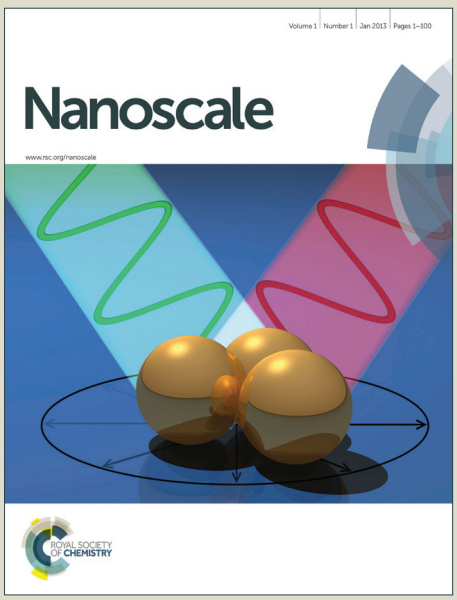

ROYAL SOCIETY OF CHEMISTRY

www.rsc.org/nanoscale

Controllable Synthesis of SnO_2@C Yolk-Shell Nanospheres as a High-Performance Anode material for Lithium Ion Batteries

Jinxiu Wang,[a] *Wei Li,*[a] *Fei Wang,*[a] *Yongyao Xia,*[a] *Abdullah M. Asiri,*[b] *and Dongyuan Zhao**[a]

[a]*Department of Chemistry and Laboratory of Advanced Materials, Fudan University, Shanghai, 200433, P. R. China. E-mail: dyzhao@fudan.edu.cn; Fax: +86-21-51630307; Tel: +86-21-51630205*

[b]*Chemistry Department and The Center of Excellence for Advanced Materials Research, King Abdulaziz University, P.O. Box 80203, Jeddah 21589, Saudi Arabia.*

Abstract

In this work, we report a facile synthesis of uniform SnO_2@C yolk-shell nanospheres as high-performance anode materials for lithium ion batteries (LIBs). The yolk-shell structured SnO_2@C nanospheres were fabricated through a two-step sol-gel coating process by using tetraethyl orthosilicate (TEOS) and resorcinol-formaldehyde (RF) as precursors, where the silica interlayer not only acts as a template to produce the void space, but also promotes the coating of RF layer. The synthesis is easy to operate and allows tailoring the carbon shell thickness and void space size. The resultant SnO_2@C yolk-shell nanospheres possess a hollow highly crystalline SnO_2 core (280-380 nm), tailored carbon shell thickness (15-25 nm) and a large void space size (100-160 nm), a high surface area (~ 205 m^2g^{-1}) and large pore volume (~ 0.25 cm^3g^{-1}), as well as a

high SnO_2 content (77 wt%). When evaluated as an anode of LIBs, the materials manifest superior electrochemical performance with a high lithium storage capability (2190 $mAhg^{-1}$ in initial discharge capacity; > 950 $mAhg^{-1}$ in the first 10 cycles), a good cycle performance and an excellent rate capability.

Key words: synthesis, yolk-shell, tin oxides, carbon, lithium ion batteries

Introduction

Lithium ion batteries (LIBs) are considered as one of the favorite energy storage devices for various portable electronics and hybrid electric vehicles in current society.[1,2] However, the energy density and cycle life of the existing batteries are insufficient to satisfy the ever-growing requirements, especially for large-scale grid storage applications. Thus it is both urgent and crucial to develop new and well-designed electrode materials because the performances of LIBs are strongly dependent on them.[3-5] For anode materials, considerable progress has been made to increase the capacities by replacing the conventional graphite with metals or metal oxides.[6-10] Among them, tin oxide (SnO_2) has attracted tremendous attention owing to its unique and fascinating properties such as a high theoretical capacity of ~790 $mAhg^{-1}$, low cost and toxicity, and widespread availability.[2,11] However, the practical implementation of SnO_2 to LIBs is greatly limited by its severe volume expansion and contraction (~250 %) during the charge/discharge process, leading to a poor cyclic stability.[12,13] Therefore, many efforts have been devoted to overcome these issues.[14-19] One of the mostly studied approaches is to construct SnO_2-based nanocomposites

based on the concept of active/inactive, in which the inactive phase serves as an effective confining buffer for the large volume change of SnO_2, thus greatly improving the cycling performances.[20] Owing to its soft nature and good electronic conductivity, carbon has been extensively used as the inactive material for integration with SnO_2 to form core-shell structures.[21-23] For example, Lou and co-workers have successfully prepared coaxial SnO_2@carbon nanospheres which exhibit a high capacity of 460 $mAhg^{-1}$ after 100 cycles at a high current density of 500 mAg^{-1}.[24] However, the carbon shells may crack and fracture due to the large volume expansion, leading to a breaking down of the core-shell structure.[25,26] As a result, the capacities of these SnO_2-carbon nanocomposites would fade quickly during cycling.

Recently, yolk-shell structure, a special core-shell architecture, has stimulated a great deal of interests because of the fascinating features including the movable cores, void space between the core and shell, and their controllability and functionality in both the core and shell.[27-32] Notably, it has been well demonstrated that the yolk-shell structure can greatly improve the cycle performances of the anode materials (such as Si, Sn and SnO_2), which possess a notorious and large volume change during the charge/discharge process.[25,26,33-36] Because the well-defined void space can not only allow the volume changes of the encapsulated electroactive cores without a collapse of the outer shells but also act as a buffering room for the electrolyte to reduce the transport length. However, to the best of our knowledge, very little success has been achieved to synthesize SnO_2@carbon yolk-shell nanocomposites with rationally designed void space and shell structure, which are highly desired as anode materials

for LIBs.

Here, we report a simple approach to synthesize uniform SnO_2@C yolk-shell nanospheres with a unique hollow SnO_2 nanoparticle encapsulated in a thin porous carbon shell, which can be used as a high-performance anode material of LIBs. The yolk-shelled SnO_2@C nanospheres were fabricated through a two-step sol-gel coating process by using tetraethyl orthosilicate (TEOS) and resorcinol-formaldehyde (RF) as precursors, where the silica interlayer not only acts as a template to produce the void space, but also promotes the coating of RF layer. This method is easy to operate and allows tailoring the carbon shell thickness (15-25 nm) and void space size (100-160 nm). The resultant SnO_2@C yolk-shell nanospheres possess a hollow SnO_2 core (280-380 nm), a thin porous carbon shell (~ 15 nm), a high surface area (~ 205 m^2g^{-1}) and large pore volume (~ 0.25 cm^3g^{-1}). More importantly, SnO_2 content is very high (~ 77 wt%) and the well-defined void space is large enough for the SnO_2 expanding freely. When evaluated as an anode of LIBs, the SnO_2@C yolk-shell nanospheres manifest outstanding performances with a high lithium storage capability, good cycle performance and excellent rate capability.

The synthesis procedure of the SnO_2@C yolk-shell nanospheres involves three steps as illustrated in Fig. 1. The first step is a Stöber sol-gel coating process, where dispersed hollow SnO_2 nanoparticles obtained from a solvothermal method[17] were firstly coated with a layer of condensed silica to produce SnO_2@SiO_2 nanospheres through the classical Stöber method using TEOS as a precursor, and subsequently coated with a polymeric layer of RF after the introduction of resorcinol and

formaldehyde, giving rise to the SnO_2@SiO_2@RF nanospheres.[37] The second step is the carbonization process under N_2 atmosphere, where the polymeric layer of RF can be converted into a carbon layer to produce SnO_2@SiO_2@C core-shell nanospheres. The third step is the silica removal, where the silica layer can be etched away by a 10 wt% HF solution to yield the final SnO_2@C yolk-shell nanospheres.

The hollow SnO_2 nanoparticles are prepared *via* a template-free solvothermal route using potassium stannate as the precursor[17] and possess uniformly spherical shape with a diameter in the range of 280-380 nm (Fig. S1). Transmission electron microscopy (TEM) image reveals the hollow structure with a shell thickness ~ 40 nm (Fig. S2). High-resolution TEM (HRTEM) image (Fig. S3) shows that the SnO_2 shells are composed of aggregated nanocrystals. Moreover, two kinds of lattice fringes with a lattice spacing of about 0.33 and 0.26 nm can also be observed, corresponding to the (110) and (101) planes of rutile type SnO_2, respectively. The SnO_2@SiO_2 nanospheres obtained after the sol-gel process of TEOS show a typical core-shell structure with a silica shell thickness of about 80 nm, as determined by the TEM image (Fig. S4). After a further sol-gel coating of RF, the obtained products preserve the spherical morphology with a slightly rough surface and have a diameter of 480-580 nm (Fig. 2a). The TEM image clearly reveals that the SnO_2@SiO_2@RF nanospheres possess a typical sandwich-like core-shell structure with a middle SiO_2 layer and an outer RF shell of ~ 20 nm (Fig. 2b). These results indicate that the silica and resin polymer RF can be successfully coated onto the hollow SnO_2 cores in turn through a sol-gel process under the typical Stöber system. Followed by the carbonization process,

FESEM and TEM images show the SnO_2@SiO_2@C nanospheres retain a similar spherical morphology and core-shell structure (Fig. 2c, d). It is worthy to note that the hollow structure of SnO_2 cores in the carbonized nanospheres becomes more clearly visible from TEM observations. The reason is ascribed to the high crystallinity of SnO_2 after calcination at a high temperature of 600 °C, which enhanced the contrast difference between the edge and centre of SnO_2 cores. After removing the silica, the obtained nanospheres can still reserve the uniform spherical morphology with a diameter of 480-580 nm (Fig. 2e). In addition, the closer examination reveals that there are many holes in the shells, which may result from the dissolution of silica layers. The TEM image (Fig. 2f) shows that the resultant SnO_2@C nanospheres possess a yolk-shell structure with one hollow SnO_2 particle attached to one side of the carbon shell. The carbon shells are very thin and the thickness is ~ 15 nm, indicating that ~ 25 % shrinkage for the RF coating layer occurs during the carbonization process. The void space is estimated to be ~ 160 nm, in accordance with the thickness of the silica coating layer. Meanwhile, the void volume is calculated to be almost three times larger than that of the encapsulated SnO_2, suggesting that the void space is large enough to accommodate the volume changes of SnO_2 during the charge/discharge process.

The X-ray diffraction (XRD) pattern (Fig. 3a) of the hollow SnO_2 nanoparticles shows ten characteristic diffraction peaks, which can be well assigned to tetragonal rutile SnO_2 (JCPDS Card No. 41-1445, space group: P42/mnm, a_o = 4.738 Å, c_o = 3.187 Å), consistent with the HRTEM results. The SnO_2@SiO_2@RF nanospheres

obtained after the sol-gel coating process exhibit a similar XRD pattern but with a reduced diffraction intensity (Fig. 3a), suggesting a negligible effect on the crystalline structure of SnO_2 during the coating process and the shielding effect of the shells. Followed by the carbonization process, apart from the well retained but more sharper diffraction peaks of crystalline SnO_2, a broad peak at 2θ value around 22° can also be observed in the XRD pattern of the SnO_2@SiO_2@C nanospheres (Fig. 3a), which can be ascribed to the amorphous carbon. Raman spectrum (Fig. S5) further show the evidence for the amorphous carbon framework, which displays two broad peaks at around 1330 and 1600 cm^{-1}, attributed to the D-band and G-band, respectively. These results implies that the carbonization process at a high temperature of 600 °C not only facilitates the RF resin polymers turn into a carbon layer, but also promotes the high crystallinity of SnO_2. After the removal of the SiO_2 layer, the obtained SnO_2@C yolk-shell nanospheres still preserve the typical diffraction peaks of crystalline SnO_2 and the broad peak of amorphous carbon (Fig. 3a). Notably, no other phase such as Sn or SnO is detected in the XRD patterns, revealing the high purity of SnO_2 in the final yolk-shell structured SnO_2@C nanospheres. It can be ascribed to the unique sandwich structure of the SnO_2@SiO_2@RF core-shell nanospheres, in which the middle silica layer prevents the direct contact of SnO_2 cores with RF shells, thus avoiding the carbothermal reduction of SnO_2 during the carbonization process even at 600 °C.

Thermogravimetric analysis (TGA) curve (Fig. 3b) of the final SnO_2@C yolk-shell nanospheres displays an obvious weight loss of 23 wt% in air in the temperature range of 300-600 °C, and the weight residue is 77 wt%. They are

attributed to the carbon and SnO_2 constituents, respectively, indicating a high SnO_2 content. The nitrogen isotherms of the yolk-shelled SnO_2@C nanospheres exhibit the mixture type IV/II curves (Fig. 3c), which is combined characteristics of mesopores and maropores, indicating a porous structure. The Brunauer–Emmett–Teller (BET) surface area and total pore volume is 205 m^2g^{-1} and 0.26 cm^3g^{-1}, respectively. It should be noted that only low detectable surface area (28 m^2g^{-1}) was observed for the SnO_2@SiO_2@C nanospheres (Fig. S6), clearly indicating that most of the surface area is produced upon the removal of silica. The pore size distribution of the yolk-shelled SnO_2@C nanospheres (Fig. 3d) derived from the adsorption branch by using the NLDFT (Nonlocal Density Functional Theory) method shows a mean pore size of ~ 3.0 nm, revealing the existence of mesopores. Furthermore, the pure hollow SnO_2 after the calcination under N_2 at 600 °C is also tested (Fig. S7). The nitrogen isotherms (Fig. S8) show the typical type-III curves with a BET surface area only ~ 18 m^2g^{-1}, which can be neglected compared with that of the SnO_2@C yolk-shell nanospheres. This result indicates that the outer carbon layer in the yolk-shell structured SnO_2@C nanospheres contributes a lot to the high surface area and large pore volume.

In this case, the size of the void space and the thickness of the carbon shells can be controlled by varying the amount of the silica and carbon precursors. For example, while the amount of the carbon precursor is kept to be constant, the thickness of the silica layer in the SnO_2@SiO_2@C core-shell nanospheres can be turned from 50 to 80 nm (Fig. S9) with increasing the amount of the silica precursor from 0.5 to 0.75 mL,

thus the size of corresponding void space can be tuned from ~ 100 to 160 nm after removing the silica layer. Furthermore, the carbon shell thickness can be increased from 15 to ~ 25 nm with the increase of resorcinol amount from 0.15 to 0.2 g and formaldehyde from 0.21 to 0.28 mL (Fig. S9). This facile synthesis approach enables the rational design and controllable synthesis of the SnO_2@C yolk-shell nanostructures. Usually, a high content of the active materials and a thin carbon shell as well as a large void space are desirable for enhancing the capacity and cycle stability. Therefore, the SnO_2@C yolk-shell nanospheres with a thin carbon shell of only 15 nm and a large void space of ~ 160 nm are further measured as an anode material for LIBs.

The cyclic voltammograms (CV) of the SnO_2@C yolk-shell nanospheres at a scan rate of 0.05 mVs^{-1} in the potential window of 3 – 0 V (versus Li/Li^+) were characterized, as displayed in Fig. 4a. Specifically, an apparent reduction peak at the potential about 0.8 V (versus Li/Li^+) is observed for the first cycle, which can be assigned to the reduction of Sn (IV) (SnO_2) to Sn (0). The peak between 0.6 and 0 V also clearly appears, arising from the formation of Li_xSn alloys ($0 \leq x \leq 4.4$). The CV profile is in agreement with that of the SnO_2 anode materials reported previously,[17,21] indicating a similar electrochemical reaction pathway. The first charge-discharge curve was measured at a constant current of 100 mAg^{-1} (0.16 C) with a potential window of 2 – 0 V (versus Li/Li^+), pure hollow SnO_2 particles after the calcination under N_2 at 600 °C were also tested for a comparison (Fig. 4b). The SnO_2@C yolk-shell nanospheres exhibit an extremely large initial discharge and charge

capacity of 2190 and 1236 $mAhg^{-1}$, respectively. The values are much larger than that (1459, 682 $mAhg^{-1}$) of the pure hollow SnO_2 particles, implying that the porous carbon shells and the void spaces can significantly improve the lithium storage. Moreover, the SnO_2@C yolk-shell nanospheres deliver a initial capacity loss of 43 %, which is lower than that (53 %) of the pure hollow SnO_2 particles, mainly attributing to the carbon coating layer and improving the conductivity of the encapsulated SnO_2.[38,39] The charge-discharge cycling performance was also evaluated as shown in Fig. 4c. As expected, this novel yolk-shell SnO_2@C nanostructure manifests a good ability to improve the cyclic performance with a high reversible specific capacity of over 950 $mAhg^{-1}$ in the first 10 cycles and a reversible capacity of ~ 630 $mAhg^{-1}$ after 100 cycles. While the capacity of the pure hollow SnO_2 particles fades quickly to a low value of only 52 $mAhg^{-1}$ after 70 cycles, suggesting that the carbon thin shells on the uniform yolk-shell structure facilitates the cycle stability. The rate performance of the SnO_2@C yolk-shell nanospheres at various charge and discharge rates in the voltage window of 2 – 0 V (versus Li/Li^+) (Fig. 4d) shows that when the current rate is first increased from 0.32 to 1 C, a stable capacity of around 630 $mAhg^{-1}$ can be achieved. Afterwards, the rate is increased stepwise up to 3.2 C, the electrode can still deliver a stable capacity of about 300 $mAhg^{-1}$. Remarkably, when the current rate is again reduced to 0.32 C, a stable high capacity of about 760 $mAhg^{-1}$ can be resumed, revealing that the SnO_2@C yolk-shell nanospheres are stable and reversible for cycling. The excellent electrochemical performance of such SnO_2@C nanospheres might be related to the unique yolk-shell structure in several aspects. First, the porous

and hollow structure offers a large electrode/electrolyte contact area, which facilitates the electrons/ions transport and surface lithium storage. Second, the large void space between the core and shell can tolerate SnO_2 expanding without cracking the carbon shell during the charge/discharge process, ensuring the integrity of the yolk-shell structure and enhancing the cycling performance. Lastly, the carbon shells are both electronically and ionically conducting and can improve the conductivity of the encapsulated SnO_2.

In summary, we have reported a facile synthesis of uniform SnO_2@C nanospheres with a well-designed yolk-shell structure. The synthesis is based on the sol-gel coating process of both TEOS and RF under the typical Stöber system, which is easy to operate and control. The resultant yolk-shell structured SnO_2@C nanospheres with uniform size (480-580 nm) possess a high crystallinity hollow SnO_2 core (280-380 nm), tailored carbon shell thickness (15-25 nm) and void space size (100-160 nm), a high surface area (~ 205 m^2g^{-1}) and large pore volume (~ 0.25 cm^3g^{-1}), as well as a high SnO_2 content (77 wt%). Most importantly, the SnO_2@C yolk-shell nanospheres exhibit an excellent performance using as an anode material of LIBs. A high initial capacity of 2190 $mAhg^{-1}$ at a current density of 100 mAg^{-1} and superior cycling performance over 100 cycles can be achieved. We believe that such yolk-shell structured SnO_2@C nanospheres with excellent electrochemical performance might be a promising material as high-performance anodes for future LIBs.

Experimental Section

Synthesis*:* The hollow SnO_2 nanoparticles were synthesized by a template-free method based on a solvothermal treatment of potassium stannate in a mixed solvent of ethanol/water at 150 °C for 24 h as described previously.[17] The core-shell structured SnO_2@SiO_2@RF nanospheres were fabricated through a simple sol-gel coating process by using resorcinol-formaldehyde (RF) as a carbon source and tetraethyl orthosilicate (TEOS) as a silica source under the typical Stöber system. In a typical synthesis, 0.10 g of the hollow SnO_2 nanoparticles was dispersed in a mixture solution containing water (20 g), ethanol (11 g), and ammonia aqueous solution (0.55 g, 32 wt%). Subsequently, TEOS (0.75 mL) was added and stirred for 0.5 h at 30 °C. Then, 0.15 g of resorcinol (R) and 0.21 mL of formaldehyde (F) solution were added with stirring. The reaction mixture was stirred for 24 h at 30 °C. Afterward, the mixture was transferred to Teflon-lined stainless steel autoclaves and hydrothermally treated at 100 °C for 24 h. The solid product of the SnO_2@SiO_2@RF core-shell nanospheres was harvested by centrifugation, washed with water and ethanol, and air-dried at 60 °C for several hours. To obtain core-shell structured SnO_2@SiO_2@C nanospheres, the SnO_2@SiO_2@RF nanospheres were heated at 600 °C for 2 h under N_2 atmosphere. For the fabrication of the yolk-shell structured SnO_2@C nanoparticles, the SnO_2@SiO_2@C core-shell nanospheres were treated with a HF solution (10 wt %) to etch the silica coating layer.

Electrochemical Measurements*:* Electrochemical tests were performed using CR2016-type coin cell. A lithium metal was used as the negative electrode. The

working electrode consisted of the active materials (e. g., the SnO_2@C yolk-shell nanospheres), conductivity agent (acetylene black), and polymer binder (polyvinylidene difluoride, PVDF, Aldrich) in a weight ratio of around 80: 10: 10. The electrolyte was 1.0 M $LiPF_6$ in a mixture (50: 50 w/w) of ethylene carbonate and diethyl carbonate. Cyclic voltammetry measurements were performed on a CHI660C electrochemical workstation. The galvanostatic charge-discharge tests were performed on a LAND CT2001A Battery Cycler (Wuhan, China) tester.

Supplementary Information

Acknowledgements

This work was supported by the State Key Basic Research Program of the PRC (2012CB224805, 2013CB934104), NSF of China (Grant No. 21210004), Shanghai Leading Academic Discipline Project, Project Number: B108, and King Abdulaziz University (KAU), under grant No. (32-3-1432/HiCi).

References:

1 J. M. Tarascon, M. Armand, *Nature*, 2001, **414**, 359.

2 J. Maier, *Nat. Mater.*, 2005, **4**, 805.

3 Y. Idota, T. Kubota, A. Matsufuji, Y. Maekawa, T. Miyasaka, *Science*, 1997, **276**, 1395.

4 C. Liu, F. Li, L. P. Ma, H. M. Cheng, *Adv. Mater.*, 2010, **22**, E28.

5 J. S. Chen, X. W. Lou, *Small*, 2013, **9**, 1877.

6 H. J. Kim, M. Seo, M.-H. Park, J. Cho, *Angew. Chem. Int. Ed.*, 2010, **49**, 2146.

7 S. B. Yang, X. L. Feng, S. Ivanovici, K. Müllen, *Angew. Chem. Int. Ed.*, 2010, **49**, 8408.

8 K. H. Seng, M. H. Park, Z. P. Guo, H. K. Liu, J. Cho, *Nano Lett.*, 2013, **13**, 1230.

9 Y. Yu, L. Gu, C. L. Wang, A. Dhanabalan, P. A. Van Aken, J. Maier, *Angew. Chem. Int. Ed.*, 2009, **48**, 1.

10 D. Deng, J. Y. Lee, *Angew. Chem. Int. Ed.*, 2009, **48**, 1660.

11 G. Derrien, J. Hassoun, S. Panero, B. Scrosati, *Adv. Mater.*, 2007, **19**, 2336.

12 M. Winter, J. O. Besenhard, M. E. Spahr, P. Novak, *Adv. Mater.*, 1998, **10**, 725.

13 D. Larcher, S. Beattie, M. Morcrette, K. Edstroem, J. C. Jumas, J. M. Tarascon, *J. Mater. Chem.*, 2007, **17**, 3759.

14 Z. P. Guo, G. D. Du, Y. Nuli, M. F. Hassan, H. K. Liu, *J. Mater. Chem.*, 2009, **19**, 3253.

15 Y. S. Huang, D. Q. Wu, S. Han, S. Li, L. Xiao, F. Zhang, X. L. Feng, *Chem. Sus. Chem.*, 2013, **6**, 1510.

16 Y. Wang, M. H. Wu, Z. Jiao, J. Y. Lee, *Nanotech.*, 2009, **20**, 345704.

17 X. W. Lou, Y. Wan, C. L. Yuan, J. Y. Lee, L. A. Archer, *Adv. Mater.*, 2006, **18**, 2325.

18 S. J. Han, B. C. Jang, T. Kim, S. M. Oh, T. Hyeon, *Adv. Funct. Mater.*, 2005, **15**, 1845.

19 L. Y. Jiang, X. L. Wu, Y. G. Guo, L. J. Wan, *J. Phys. Chem. C*, 2009, **113**, 14213.

20 A. S. Aricò, P. Bruce, B. Scrosati, J. M. Tarascon, W. Van Schalkwijk, *Nat. Mater.*,

2005, **4**, 366.

21 X. W. Lou, D. Deng, J. Y. Lee, L. A. Archer, *Chem. Mater.*, 2008, **20**, 6562.

22 Z. Wang, Z. Wang, S. Madhavi, X. W. Lou, *J. Mater. Chem.*, 2012, **22**, 2526.

23 J. Liu, W. Li, A. Manthiram, *Chem. Commun.*, 2010, **46**, 1437.

24 X. W. Lou, C. M. Li, L. A. Archer, *Adv. Mater.*, 2009, **21**, 2536.

25 N. Liu, H. Wu, M. T. Mcdowell, Y. Yan, C. M. Wang, Y. Cui, *Nano Lett.*, 2012, **12**, 3315.

26 W. M. Zhang, J. S. Hu, Y. G. Guo, S. F. Zheng, L. S. Zhong, W. G. Song, L. J .Wan, *Adv. Mater.*, 2008, **20**, 1160.

27 W. Li, Y. H. Deng, Z. X. Wu, X. F. Qian, J. P. Yang, Y. Wang, D. Gu, F. Zhang, B. Tu, D. Y. Zhao, *J. Am. Chem. Soc.*, 2011, **133**, 15830.

28 J. Liu, S. Z. Qiao, S. B. Hartono, G. Q. Lu, *Angew. Chem., Int. Ed.*, 2010, **49**, 4981.

29 Y. J. Hong, M. Y. Son, Y. C. Kang, *Adv. Mater.*, 2013, **25**, 2279.

30 M. Hu, A. A. Belik, M. Imura, Y. Yamauchi, *J. Am. Chem. Soc.*, 2013, **135**, 384.

31 L. Wang, Y. Yamauchi, *J. Am. Chem. Soc.*, 2013, **135**, 16762.

32 C. L. Li, Y. Yamauchi, Y. Yamauchi, *Phys. Chem. Chem. Phys*., 2013, **15**, 3490.

33 J. Liu, Y. C. Zhou, J. B. Wang, Y. Pan, D. F. Xue, *Chem.Comm.*, 2011, **47**, 10380.

34 A. Q. Pan, H. B. Wu, L. Yu, X. W. Lou, *Angew. Chem. Int. Ed.*, 2013, **52**, 1.

35 L. Zhou, D. Y. Zhao, X. W. Lou, *Adv. Mater.*, 2012, **24**, 745.

36 K. T. Lee, Y. S. Jung, S. M. Oh, *J. Am. Chem. Soc.*, 2003, **125**, 5652.

37 W. Li, D. Y. Zhao, *Adv. Mater.*, 2013, **25**, 142.

38 M. S. Park, G. X.Wang, Y. M. Kang, D. Wexler, S. X. Dou, H. K .Liu, *Angew.*

Chem. Int. Ed., 2007, **46**, 750.

39 R. Demir-Cakan, Y. S. Hu, M. Antonietti, J. Maier, M. M. Titirici, *Chem. Mater.*, 2008, **20**, 1227.

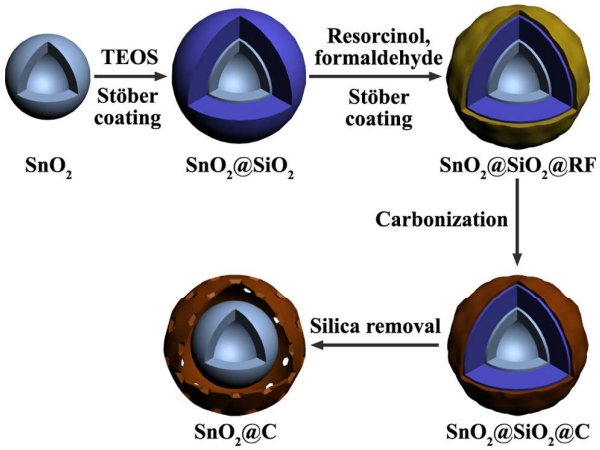

Fig. 1 Schematic illustration of the formation process of the SnO_2@C yolk-shell nanospheres.

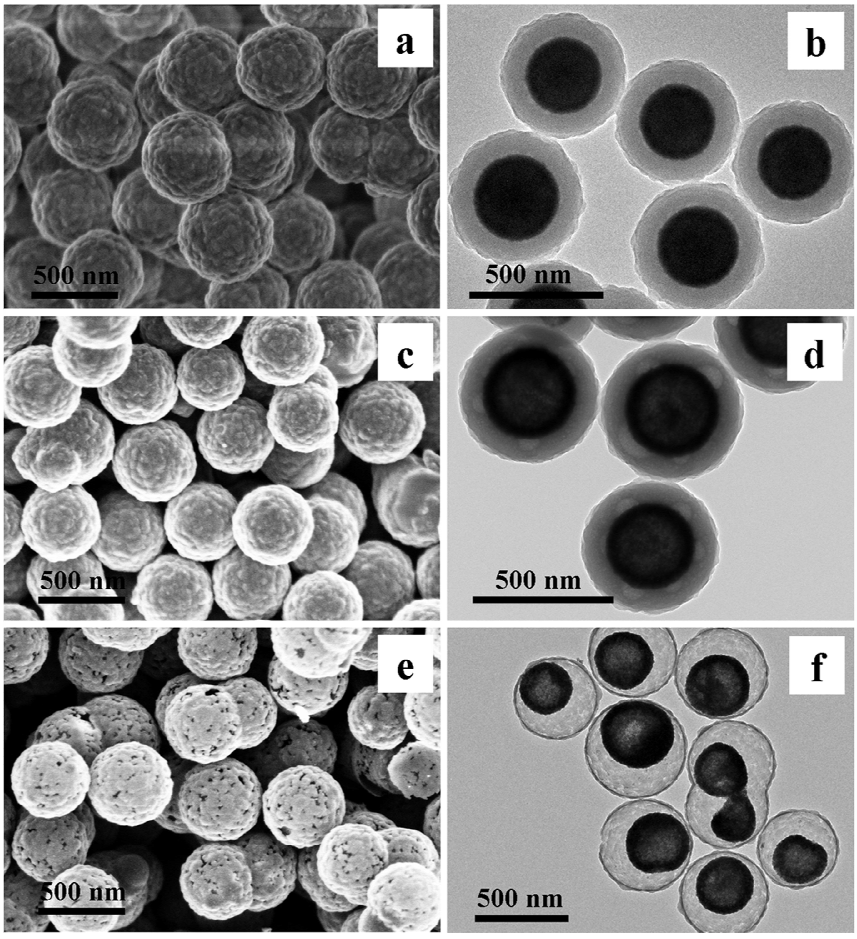

Fig. 2 a) FESEM and b) TEM images of the SnO_2@SiO_2@RF core-shell nanospheres; c) FESEM and d) TEM images of the SnO_2@SiO_2@C core-shell nanospheres before the removal of the silica layer; e) FESEM and f) TEM images of the SnO_2@C yolk-shell nanospheres.

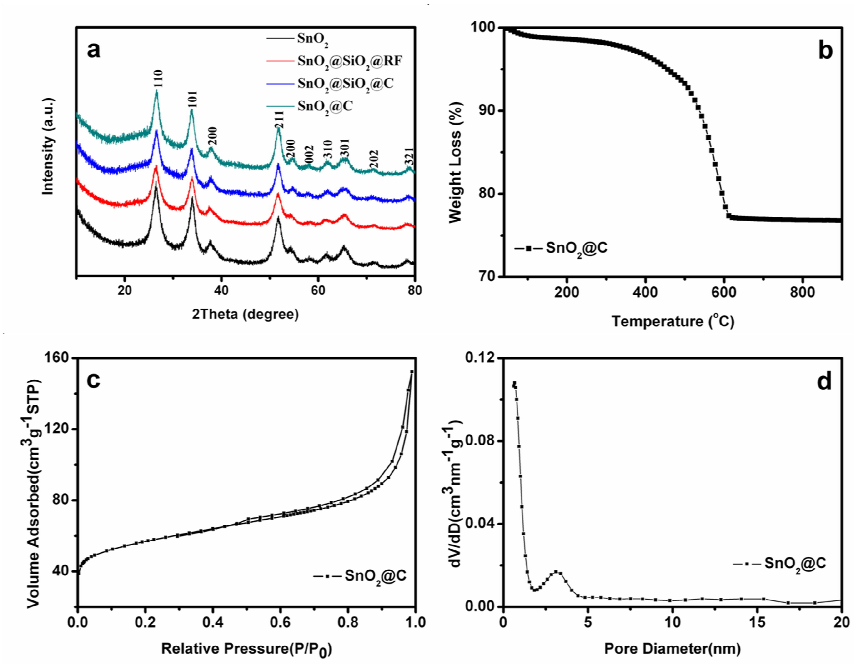

Fig. 3 a) XRD patterns of the hollow SnO_2 nanoparticles, SnO_2@SiO_2@RF core-shell nanospheres, SnO_2@SiO_2@C core-shell nanospheres before the removal of the silica layer and SnO_2@C yolk-shell nanospheres; b) the TGA curve of the SnO_2@C yolk-shell nanospheres, recorded in air; c) N_2 sorption isotherms and d) pore size distribution of the SnO_2@C yolk-shell nanospheres.

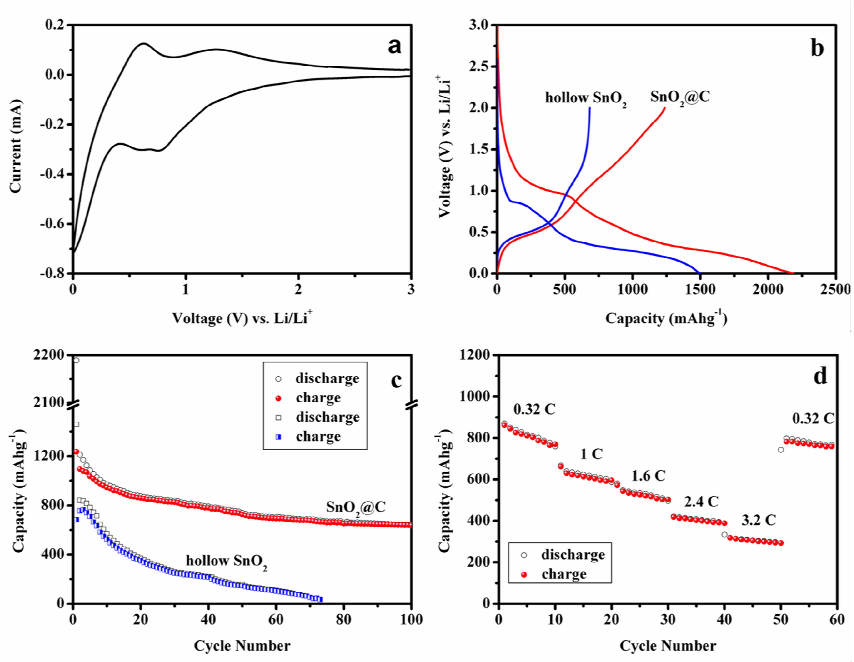

Fig. 4 a) First CV curve of the SnO_2@C yolk-shell nanospheres; b) First discharge-charge curves and c) cycling performances of the SnO_2@C yolk-shell nanospheres and pure hollow SnO_2 particles obtained after the calcination under N_2 at 600 °C; d) Rate capability of the SnO_2@C yolk-shell nanospheres at different current densities (1C = 625 mAg^{-1}).

Colour graphic:

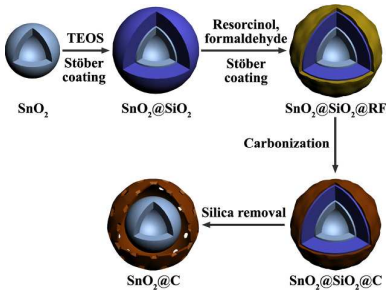

Text: Uniform SnO_2@C yolk-shell nanospheres as high-performance anode materials for lithium ion batteries